Solid Freeform Fabrication 2017: Proceedings of the 28th Annual International Solid Freeform Fabrication Symposium – An Additive Manufacturing Conference
Reviewed Paper

MULTISCALE ANALYSIS OF CELLULAR SOLIDS FABRICATED BY EBM

Edel Arrieta [a, *], Jorge Mireles [a, c], Calvin Stewart [a], Cesar Carrasco [a, b] and Ryan. B. Wicker [a, c]

[a] The University of Texas at El Paso, El Paso, TX 79968 USA.
[b] Future Aerospace Science and Technology Center (FAST), The University of Texas at El Paso, El Paso, TX 79968 USA.
[c] W.M. Keck Center for 3D Innovation, The University of Texas at El Paso, El Paso, TX 79968 USA.

[*] Corresponding author.
e-mail: egarrieta@miners.utep.edu (*E. Arrieta*)

Abstract

Additive Manufacturing technologies such as Electron Beam Melting are empowering individuals to develop novelty materials by introducing hierarchical levels into solids. Features from the introduced architectures and the manufacturing technology grant these metamaterials with mechanical performances not commonly seen in standard solids. Thus, the response of cellular metals can now be manipulated. In general, the reported research on lattices focuses on very specific topics such as microstructure, geometry and orientation, giving the impression of isolated knowledge. However, the response of these metamaterials is the result of a complex multiscale interaction between these and other factors ranging from the microstructure of the constitutive solid, up to the cell topology. Intended as a one-stop introductory document for a new branch of material designers, the major factors affecting the response of cellular metals are identified, classified and merged into a multiscale discussion supported with evidence from a series of experiments including ASTM standard tests of EBM Ti-6Al-4V standard and lattice specimens, accompanied by failure analysis. The testing features digital image correlation (DIC) for measuring deformations, strain fields, as well as Poisson and shear effects, becoming a critical tool for the advanced characterization of specimens, especially those with complex geometries that normally would require specific instrumentation. Among these multiple determinants; microstructure, manufacturing orientation, manufacturing process, Maxwell's stability criterion, and other geometrical features are discussed for the comprehensive understanding of two lattice designs presented herein. Lastly, Illustrative examples of how the stress-strain curves are helpful in diagnosing design features to start reverse engineering processes, and a summary of the determinants effects are included.

Keywords

Cellular solids; unit-cell; EBM Ti-6Al-4V; digital image correlation; microstructure.

1. Introduction

Although relatively new, cellular metal solids have proved possessing new and unique properties such that they can be classified apart from the existing materials. Typified mainly by lower densities than the standard constitutive solid metal they are made from, the cellular metals display peculiar properties such as mechanical, thermal, electrical, acoustical and electromagnetic that can be combined to serve as multifunctional structures (Figure 1).

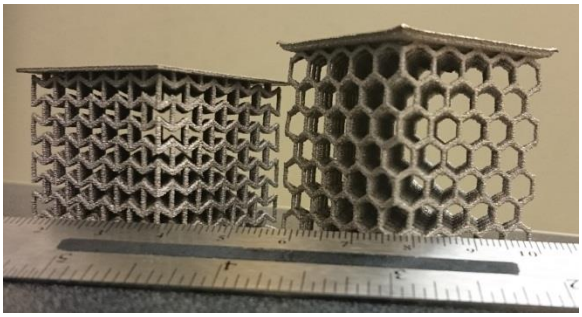

Figure 1 Two designs of EBM Ti-6Al-4V cellular solids fabricated by The W.M. Keck Center for 3D Innovation ("W.M. Keck Center for 3D Innovation," n.d.).

The introduction of hierarchical levels within the constituent solid metal creates cellular solids with special characteristics and performance not seen in standard solid metals. Among additive manufacturing (AM), the powder bed fusion technologies such as selective laser melting (SLM) and electron beam melting (EBM), mainly, permit the introduction of these hierarchical levels in a structured manner, thus potentially exerting control on the performance of the cellular solid. Manufacturing parameters and processes inherently grant attributes to the microstructure of the constituent solid; however size restrictions and technology issues are still impeding from delivering microstructural features in a more precise and localized manner; as a result, the characterization of cellular solids still lacks in accuracy. The complexity in characterizing these materials results from the combined effect of multiple determinant factors, the interaction between each other, and its influence through different scale levels. This work analyzes and classifies these identified aspects, with accompanying experimental evidence from experiments over different EBM Ti-6Al-4V specimens, including: ASTM E8 standard compression of metals, ASTM E9 standard tension of metals, tension of microstruts and compression of cellular lattices.

2. Overview

This document is based on non-stochastic cellular Ti-6Al-4V fabricated by EBM, with particular interest to deliver comprehensive understanding on these materials, for the conscious development of energy absorption applications. Although some experiments herein are not exclusively on cellular lattices, their findings are supporting evidence that the manipulation of the determinant factors, in which this analysis is subdivided for its presentation, influence the

properties of the constitutive solid, and therefore the response of the cellular metal. For these purposes, a variety of specimens, initially drafted in Solidworks, is fabricated using Arcam AB Ti-6Al-4V prealloyed precursor powder with spherical particle size distribution from 40-100μm (Figure 6), in an Arcam A2 system, with Arcam AB's standard parameters for 50μm layers. The standard parameters consist of a pre-heat step taking place to maintain the fabrication environment at approximately half of the material's melting point (~700-760°C for Ti-6Al-4V). Powder within the fabrication environment is deposited using a raking mechanism and selectively melted using a current of 18mA max with beam speeds of 500-1,000mm/s. The process takes place in a high vacuum environment of up to 10-5mBar and repeated layer-by-layer from the preheat step until fabrication is complete. The list of specimens fabricated at different build angles (Figure 2) includes:

- 0.8 x 0.8x70mm microstruts at 0°, 30°, 45°, 60° and 90°. With a specimen count of 14, 14, 3, 8 and 7pcs, respectively.
- ASTM E8 standard tension test cylindrical specimens with gauge length and diameter of specimens 40mm and 6mm respectively, fabricated at 0°, 30°, 60° and 90°. Three specimens of each orientation.
- ASTM E9 cylindrical standard compression test specimens with a diameter of 11.7mm and 23.5mm in length are fabricated at 0°, 30°, 60° and 90°. Three specimens of each orientation.
- 3D lattices at three different densities based on unit-cell sizes of 5mm, 6mm, and 7mm, lattices are composed by 5 x 5 x 5 unit cells formed by 0.8mm x 0.8mm square section microstruts; all nominal dimensions. Three specimens of each density, in two different unit-cell configurations, for a total of 18 lattice specimens.

The unit-cells variants forming the lattices are hexagonal and re-entrant hexagonal for the investigation of negative Poisson's effect. The lattices are fabricated with an integrated bearing plate of 1mm nominal thickness to guarantee uniform stress distribution and avoid damaging the compression platens (Figure 3).

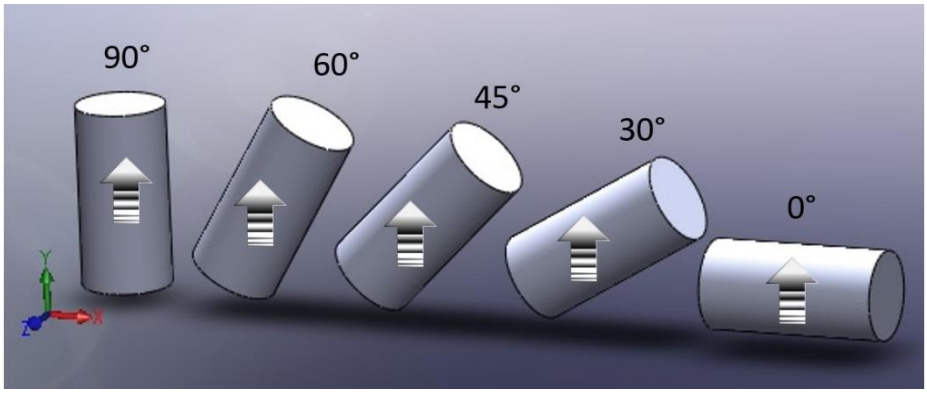

Figure 2 Representation of different build angles. XZ defining the powder bed plane, arrowheads indicating building direction (vertical, parallel to the beam), and hatch representing the layering pattern.

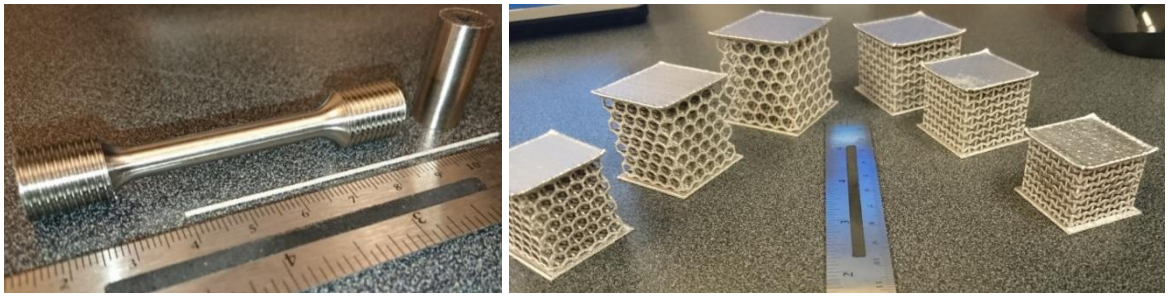

Figure 3 ASTM E8, ASTM E9 and microstrut specimens (left). Hexagonal and reentrant hexagonal lattices in 5, 6, and 7mm unit-cell sizes each.

The microstruts were tested under tension in an ADMET MTEST Quattro system with an installed load cell capacity of 1,000lbf and crosshead speed controlled at 0.003mm/mm/min; avoiding any wrongful data from the slipping at the grips, the strain was measured using a digital image correlation (DIC) system and VIC-gauge software, both from Correlated Solutions (CS). The tension test specimens were tested according to ASTM E8 standard in an Instron 5969 UTM with an installed load cell capacity of 50kN and crosshead speed set to an equivalent strain rate of 0.003mm/mm/min; strain was measured with a 25.4mm axial clip extensometer and backed up by DIC, serving also for its validation (Figure 4). The compression test specimens were tested according to ASTM E9 standard in an Instron 5594 UTM with an installed load cell capacity of 100ksi and equipped with 9in compression platens with spherical seat; a crosshead speed of 0.003mm/mm/min was set, and strain is measured by DIC using the Vic-3D software from CS. The compression tests on the lattice specimens were conducted in an MTS Landmark 370 servo-hydraulic test system with an installed load cell capacity of 100kN, equipped with MTS 643 compression platens with spherical seat; a crosshead speed of 0.003mm/mm/min was used, and strain was also measured by DIC using the Vic-gauge software. The orientation and identification of specimens were of special attention and preserved at all times.

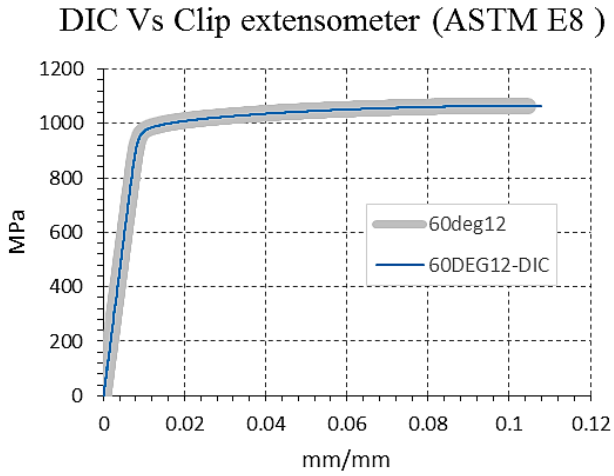

Figure 4 Axial strain measured with virtual (thin line) and clip extensometer (thick line).

The design and fabrication of cellular materials need to be proposed to be analyzed as a multidimensional optimization problem, where the limits need to be known and the variables constrained, or statistically approached. The experiments listed in this overview section allowed identifying features that can influence the performance of the cellular metals; these findings are discussed and classified according to scale for a structured way of thinking, and insight about a designing process for cellular metal solids that still will be required of the development of quantitative expressions. In this context, features granted from the manufacturing technology and material microstructure, mostly, take their place at a *microscale* level; characteristics close to the size of the unit-cell such as shapes, cell orientation, and topology, among others are considered at a *mesoscale* level, whereas the *macroscale* level analyses are upon the performance of the cellular solid (Figure 5).

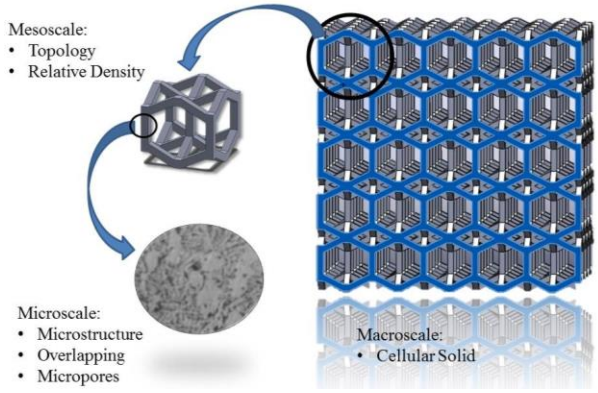

Figure 5 Overview of the scale levels in the analysis of cellular solids.

3. Microscale

Size restrictions result in limited control and flexibility in the design features that can be granted at this scale. These features range from surface roughness up to atomic structures, however, the control to delivering these to convenient regions in the lattices is very modest. The determinants at this level include manufacturing technology, file format, constituent solid, manufacturing parameters, manufacturing process, and mechanical properties degradation.

3.1. Manufacturing technology

EBM and SLM may be considered two of the most convenient AM techniques for the structured fabrication of cellular metals, and each technology could grant these metametals different characteristics. The higher beam energy in the EBM compared to the SLM process normally produces builds with lower residual stress and coarser surfaces, originating stress

concentrators that become critical as the cross section area of the microstruts decreases (Cheng et al., 2012; Hernández-Nava et al., 2016; Murr et al., 2009). Normally, Ti-6Al-4V components fabricated by EBM display larger amounts of the more ductile α-phase (Hexagonal Close Packed) microstructure than those by SLM, displaying more of the α'-phase microstructure (Murr et al., 2009). Additionally, the atmosphere in the manufacturing chamber, and the availability and characteristics of the precursor powders from each manufacturer, such as the particle size distribution and chemical composition have an influence on the efficiency of the beam, the purity and the physical and chemical characteristics of the solidified builds (Wang et al., 2014). In general, the selection of precursor powder and technology is subjected to availability.

3.2. File format

The stereolithography (.STL) file format is currently the common file for additive manufacturing systems. This format describes volumetric objects by representing only their surfaces, which in turn are discretized into planar triangles exclusively. The layering discretization approach from the AM technologies combined with the geometric representation of planar triangles, that also neglects color and texture can reduce the flexibility of design, and potentially introduce flaws and defects in the components. In this context, if significant inaccuracies compromising the component are produced, these can be addressed by overdesigning, until a more precise format such as the Additive Manufacturing File (AMF), or any other, is fully developed and becomes a new standard. (Paul and Anand, 2015).

3.3. Constituent solid

Properties from the constituent solid directly contribute to the performance of lattices and foams, where the mechanical, thermal, electrical, and other properties from the constituent are directly granted to the cellular solid. Therefore, it is most likely that a brittle constituent will produce unit-cells that also fail brittle, and similarly for ductile solids.

Having in mind the premise that *no medium is, in reality, a continuum*, atomic structures in the constituent solid material could also be recognized to deform as either mechanisms or trusses, more than as a continuum solid (refer to 4.4). Thus, the mechanical response of the cellular metals can be tailored by combining the deformation mechanisms of the unit-cells and that of crystalline structures, at the mesoscale and microscale respectively. In that context, the capability to deform as a mechanism, in the elastic range, (van der Giessen, 2011) of the 3D hexagonal honeycomb unit-cell could be enhanced if it is fabricated utilizing solids with a generous amount of Hexagonal Close Packed (HCP) atomic structures that could be seen to deform also as mechanisms, such is the case of α-phase titanium. Otherwise, the deformation capability of the unit-cell can be reduced if fabricated with constituent solids with predominantly rigid crystalline structures such as β-phase titanium, to exemplify our material selection.

The spatial concepts of allotropy could also apply in understanding the development of alloys, where a different element is introduced in the base crystalline structure to reconfigure it and alter its physical properties. For the powder bed fusion technology, the availability of prealloyed powders should be considered, as well as its particle-size distribution. It is also important to have in consideration the number of life cycles of the reclaimed powder given that, from the previous cycles, some particles could have been fused to each other, besides suffering alterations in their microstructure, originating abnormal shapes that can result in flaws and defects (Figure 6). Thus, in reducing the variability of the physical properties due to the powder precursor, the quality and size distribution of the particles shall be maintained as uniform as possible. Additionally, it has been observed that the coarseness of the surface is close to the order of the size of the smallest particles. (Hernández-Nava et al., 2016).

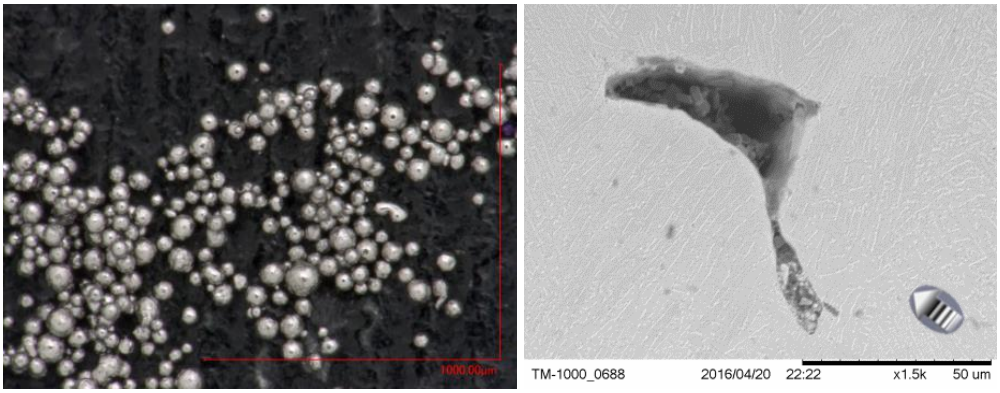

Figure 6 Prealloyed ARCAM Ti1-6Al-4V with some sintered particles; 1mm scale mark (left). A flaw in a 30° standard tension specimen; unmelted material and rounded shapes of partially melted particles are observed; 50µm scale mark (right).

3.4. Manufacturing parameters

Some of the main differences between SLM and EBM are the type and the intensity of the beam energy, as well as the manufacturing atmosphere, however, most of the effects due manufacturing parameters of these two technologies are comparable. It is of special attention that SLM and EBM are capable of producing a variety of material phases by controlling manufacturing settings (Murr et al., 2012).

The optical micrographs of the specimens, fabricated with the parameters previously described, revealed a microstructure with no visible features due the layering fabrication and a bi-modal uniform distribution of α and β-phase titanium, plenty of acicular phase, suggesting the reason for the large elongations obtained from the tensile test (Figure 7Figure 13).

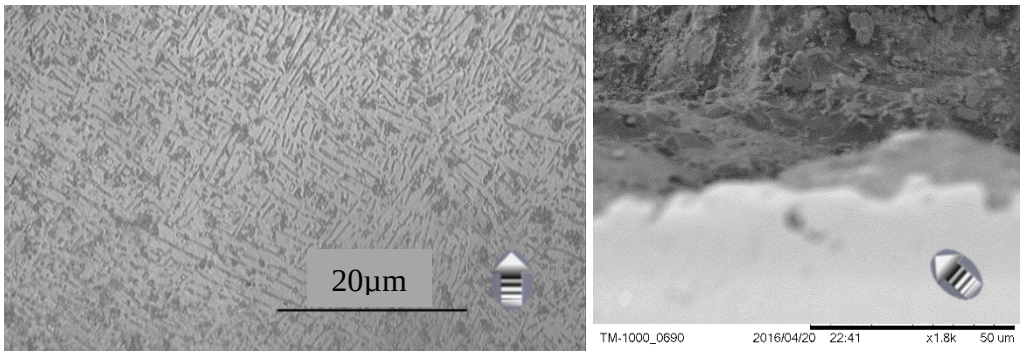

Figure 7 Bi-modal microstructure with uniformly distributed acicular, α-phase (HCP) surrounded by the stiffer β-phase (dark) (BCC) in Ti-6Al-4V cylindrical rods at 90° (left). Fracture surface at perspective displaying ductile features such a prominent crest and dimples; 50µm scale mark (right)

Manufacturing parameters such as the layering thickness and beam power have direct effect on the small cross sectional areas of microstruts and the density of the material; thin layers and high beam power will tend to produce a nearly fully dense material, minimizing the presence of unmelted, sintered powder, and pores that might act as critical stress concentrators (Figure 8) (Gong et al., 2013). Similarly, longer exposure times will produce larger and more uniform melting pools, resulting in denser solids. Thus, occurrence of internal flaws, the uniformity of the surfaces, and properties of the builds are directly affected by the manufacturing time and energy spent during fabrication (Tsopanos et al., 2010). The microstrut specimens taking part in this study were fabricated with nominal dimensions of 0.8mm x 0.8mm x 70mm; however, their cross-section was barely noticeable as squared and clearly not constant along the microstrut (Figure 9).

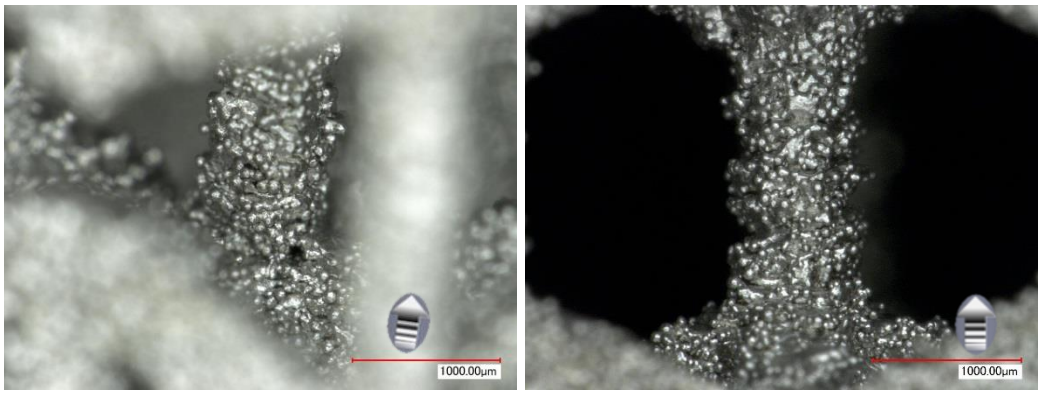

Figure 8 Void at one of the internal nodes in a reentrant hexagonal lattice (left). Profile of an internal microstrut in a hexagonal lattice (right). 1mm scale marks.

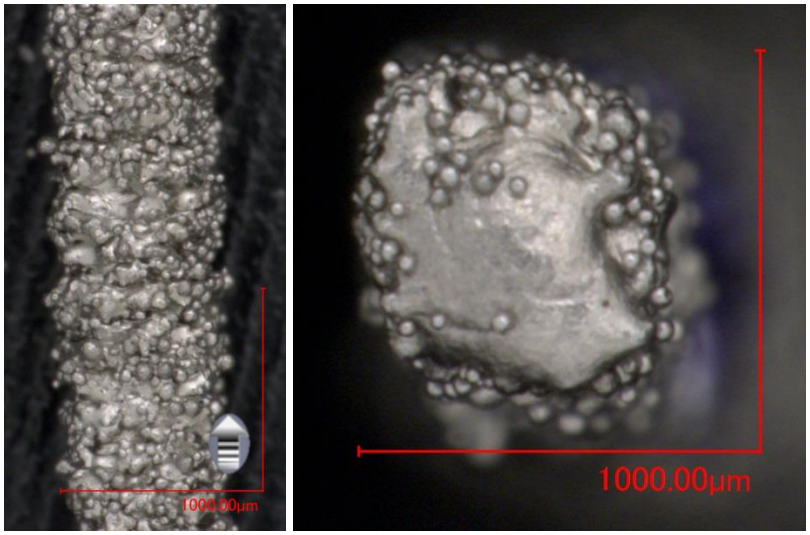

Figure 9 Profile and top view (left and right) of a 90°, 0.8mm x 0.8mm square microstrut.

3.5. Manufacturing process

Cooling and solidification rates are dependent of multiple factors; they are affected by the manufacturing parameters, the manufacturing layout of components being fabricated, and the geometry of the component itself, and that includes any support required for its fabrication. These rates have been found to alter the microstructure, phases and grain sizes in Titanium alloys. (Cansizoglu et al., 2008; Murr et al., 2010)

The different material densities constantly created throughout the manufacturing space, the building strategies considering the spatial position, and the orientation and number of builds being fabricated produce different thermal gradients that can alter microstructures and therefore material properties. This effect is more noticeable in bodies with a large area to volume ratio such as the case of the microstruts fabricated individually. Although individual microstruts for tension were fabricated from the same CAD file and manufacturing settings, the strength of the microstruts displayed variability between batches, suggesting their higher sensibility to the thermal gradients due the different components layout and its location within the manufacturing space (Figure 10).

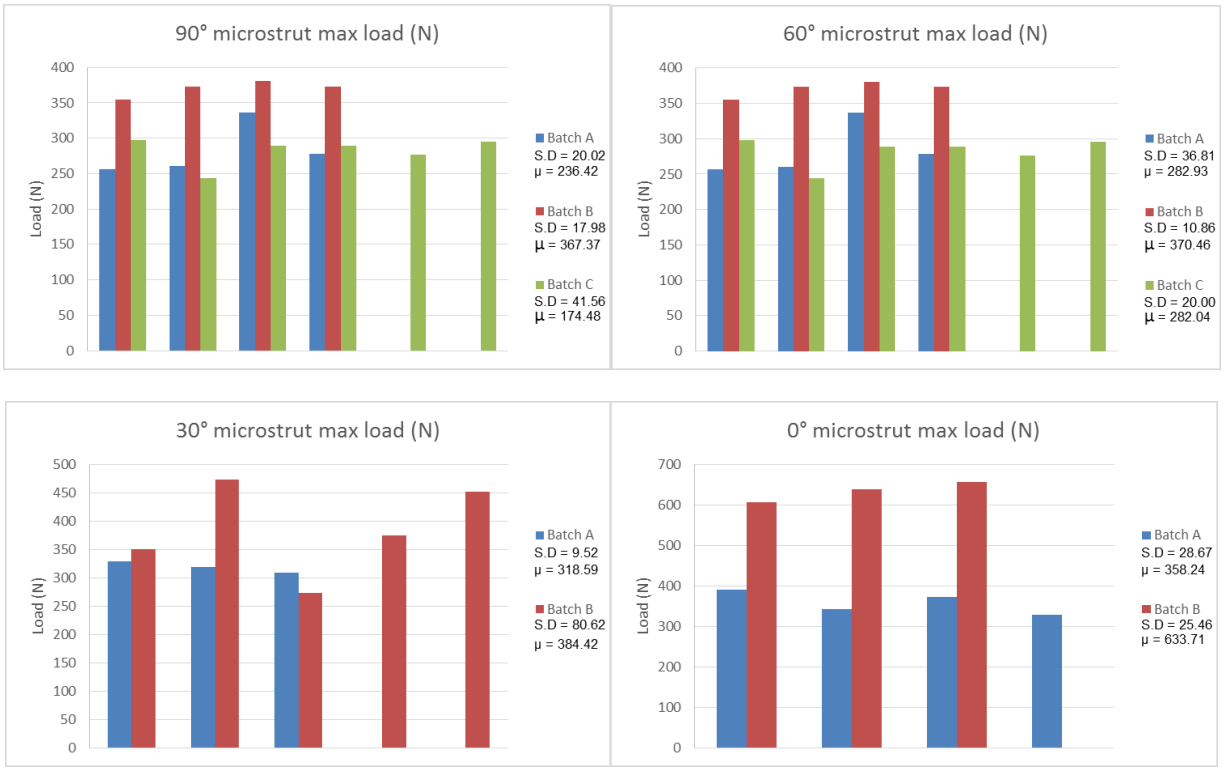

Figure 10 Strength variability between batches of microstruts with different orientations.

As a consequence of the layering process proper from the powder bed fusion, the quality of the microstrut surface is affected to great extent by the layer thickness and the build angle (Figure 11), threatening its integrity as the area of the microstrut decreases and the slenderness ratio is increased. Therefore, it is important to pay especial attention to the location of components sensitive to manufacturing orientation and thermal stresses when optimizing the manufacturing space in the chamber, besides the layer thickness analyzed as a manufacturing setting.

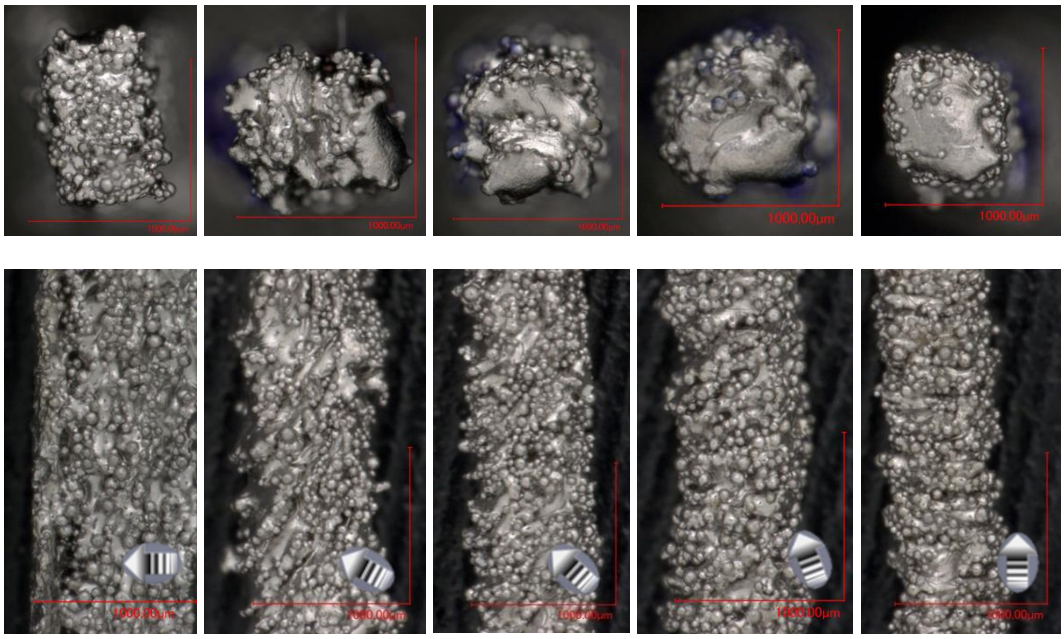

Figure 11 From left to right: 0°, 30°, 45°, 60° and 90° microstruts top and lateral views displaying layering striations with partially melted particles.

On the build angle; the microstructure in the standard tension test specimens was uniform with no trace of the interface between layers (Figure 7), however the failure profiles of the four orientations studied presented different failure modes. It is of special attention that those specimens with symmetrical layering with respect to the axial loading failed similarly; the fracture features such as a slight necking, shear lips, and failure planes normal to the main stress are well defined and characteristic of a flat-face failure mode; a mode that is related to a triaxial tensile-stress system corresponding to a planar strain state. Whereas in the profiles of the specimens fabricated at 30° and 60°, the fracture features in the profile were not defined with the same clarity, possibly indicating some shear effect (Figure 12). Although the uniformity in the microstructure suggested that the interface between layers does not represent a major source of shear strains for the 30° and 60° specimens, the presence of oriented flaws (Figure 13) could develop stress concentrations with orientations other than the principal stress, leading to the shear strains that the failure profiles suggest. Again, a reminder that the spatial location and orientation of the components might result in favorable, or unfavorable performances, according to the intended application of the component.

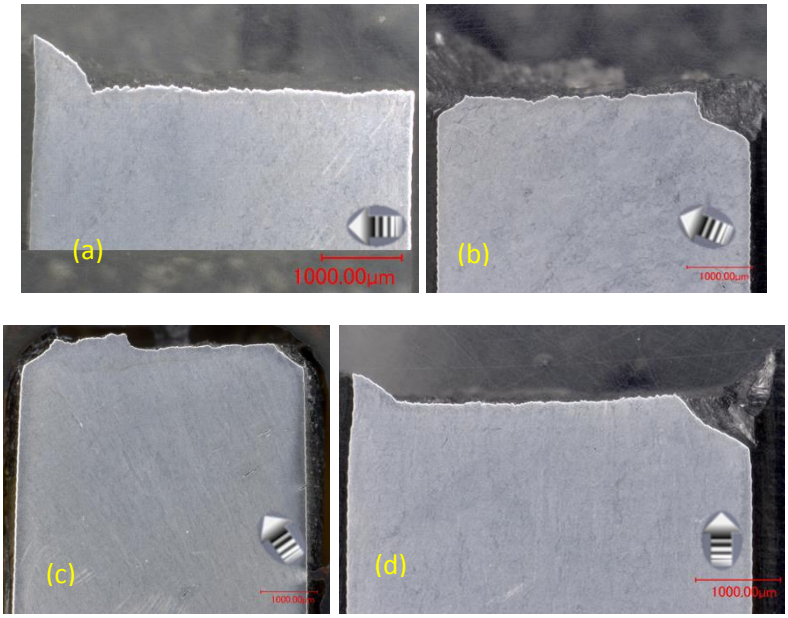

Figure 12 Failure profiles of 0°, 30°, 60°, 90° (a, b, c, d respectively) standard tension specimens displaying necking and shear lips for 0° and 90°, both, characteristics of ductile flat-face tensile failures. 1mm scale marks.

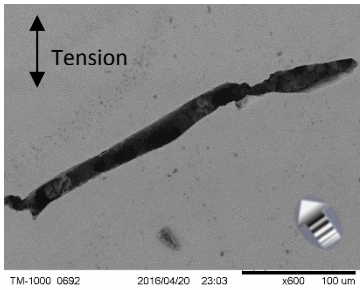

Figure 13 Flaw in a 60° standard tension test specimen; notice that a build angle is 60° and consequently the flaw is oriented 30° from the horizontal. 100µm scale mark.

Manufacturing settings and process can be managed to develop specific, localized behaviors, as well as convenient energy managing failure modes that could be advantageous for the performance of AM components over those traditionally fabricated. Thus, in an experiment with one of the tension test specimens, it was possible to fabricate similar Ti-6Al-4V components with similar strengths but displaying dissimilar performances: one with long plastic regions, and another emulating a purely brittle material failure, like glass (Figure 14). The brittle-like failure with similar strength was made possible in the component by interrupting its building process, noteworthy is the ability to localize the fracture along the component by stopping the process (Mireles, 2016). The fractography of the specimen revealed a mixture of ductile and brittle features in the same fracture surface (Figure 15). The weaker bonds between sintered powder particles

originated the brittle features, resulting in an induced lower toughness, but similar strength. Moreover these intentionally introduced flaws, it is important to monitor those accidentally introduced, such as those due electromagnetic disturbances produced by in manufacturing areas.

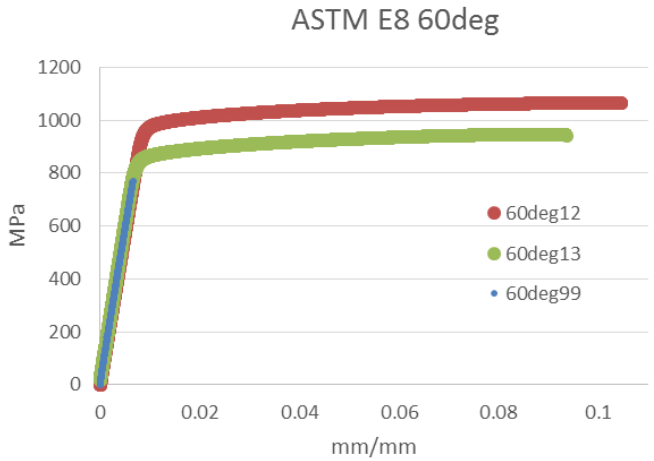

Figure 14 Stress-strain of 60° tensile specimens. 60deg99 representing the specimen with an interrupted building.

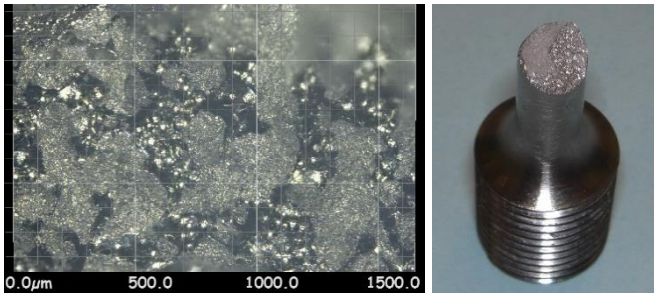

Figure 15 Fractography with mixed ductile and brittle features in a tensile specimen with interrupted building process; 500µm scale grid (left). Failed specimen (right).

The lower variability of the compressive strength compared to the tensile strength of specimens is an indicator of the larger sensitivity of the metal to flaws and defects, under tension (Figure 16 and Figure 17); this could be explained by the stress alleviation mechanism over the internal surfaces in the flaw when the gap closes due compression, compared to the infinite stress concentration at the sharp ends of the flaw when loaded under tension (Figure 18). The comparably similar average strength under tension and compression supports the assumption made about similar tensile and compressive behaviors of the Ti-6Al-4V, when obtaining the response from testing individual microstruts for the future characterization of lattices. The buckling and eccentricities developed in the microstruts in the cellular metal may be addressed most likely as geometric features under the mesoscale.

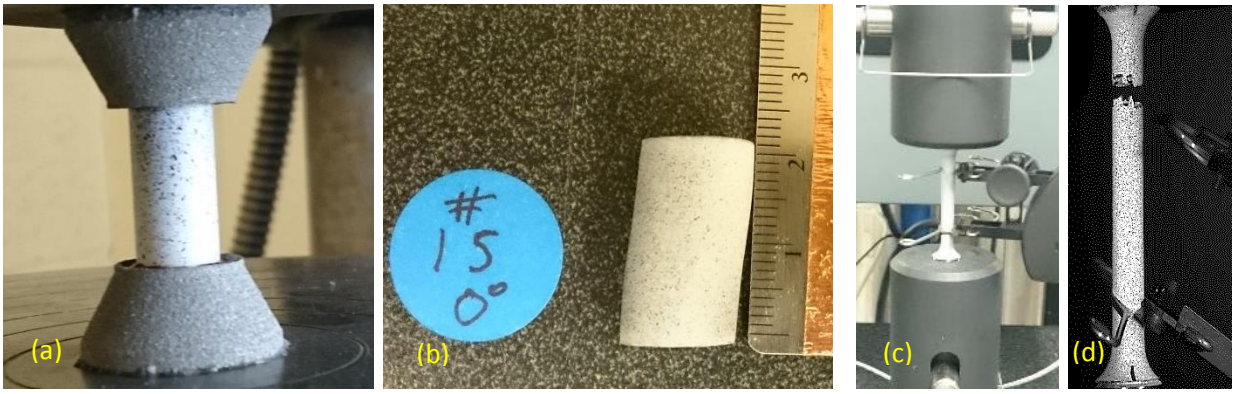

Figure 16 Setup and failed specimens under compression and tension (a, b and c, d).

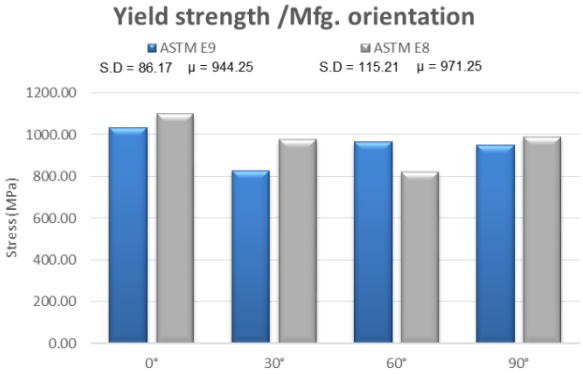

Figure 17 Average and standard deviation of tensile and compressive yield strengths on specimens at different orientations.

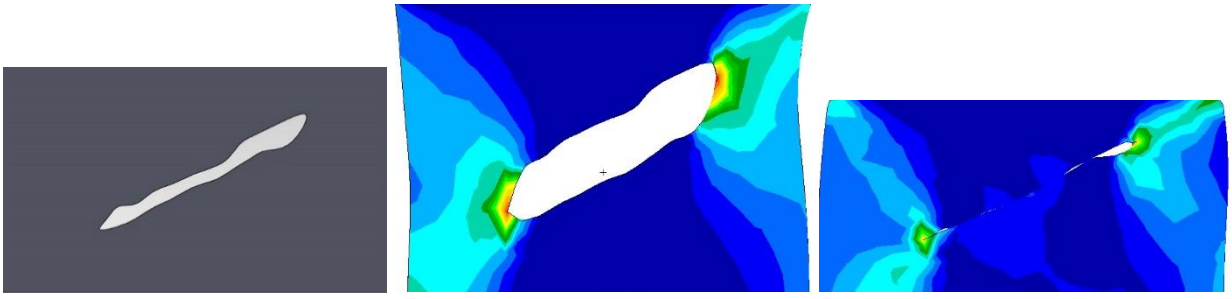

Figure 18 FEM of a flaw (left). Under tension, plastic strain concentrates at the ends of the flaw until rupture, while material in dark blue is inefficiently stressed (center). Under compression, the relief of plastic zones after the gap closes and stress redistributes along the gap (right).

3.6. Degradation of the Mechanical properties

The implicit step-like features from powder bed fusion fabrication incorporate geometrical inconsistencies or inaccuracies. This yields to the degradation of properties, mechanical and others that are dependent of the build angle and layer thickness, mostly. Regardless of the flaws and defects addressed in the manufacturing process, the deterioration of the mechanical properties shall be considered, especially, when designing components with large perimeter to area ratios, such as the microstruts forming lattices. The small cross-sectional areas in the microstruts exposed the sensitivity of its tensile elastic modulus to the manufacturing orientation (Figure 19); besides, smaller cross-sections result in microstruts with higher slenderness ratios, and thus, more susceptible for elastic buckling failure, under compression. If the degradation of the elastic modulus is considered to be attributable only to the reduction of the cross-sectional area along the microstruts, resulting from the step-like features, the effective cross-section area is estimated to be approximately 75% of the nominal area (0.8mm x 0.8mm), thus an indirect measurement of the effective area is suggested for small components. Counterintuitive to the assumption that lower build angles represent smaller layer overlaps, diminishing the effective cross-section, the microstruts fabricated at low angles showed to be stiffer under axial tensile test (Figure 20). This can be explained by the consistent larger cross-section of the 0° microstruts, and the layers overlapping all along themselves, parallel to the load. In the 90° microstruts, the layers are stacked perpendicular to the load, thus a triaxial stress state is rapidly developed in planes weakened by external flaws and surface imperfections reducing the effective cross sectional area and resulting in lower strengths. Whereas on the 30° and 60° microstruts, the loading is alleviated by principal stresses, but also by shear stresses potentially developed from rotational deformations of each layer due to the asymmetry of the surface stress concentrators, eccentricity and loading being transferred oblique to the overlaps, where the weakest plane most likely exists (Figure 11 and Figure 21).

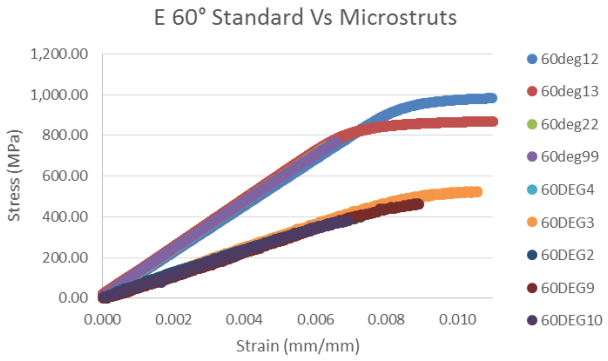

Figure 19 The elastic modulus of 60° Ti-6Al-4V calculated for 0.8mm x 0.8mm microstruts is over 25% lower than that for the standard tension test specimens (116Gpa approx.).

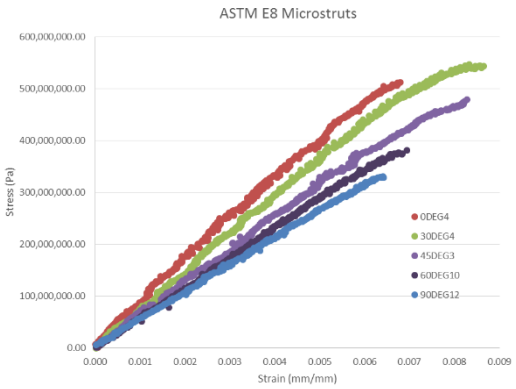

Figure 20 Stress-strain curves of 0°, 30°, 45°, 60° and 90° microstruts. Microstruts fabricated at lower build angles showed to be stiffer and stronger. All orientations observed a practically linear response.

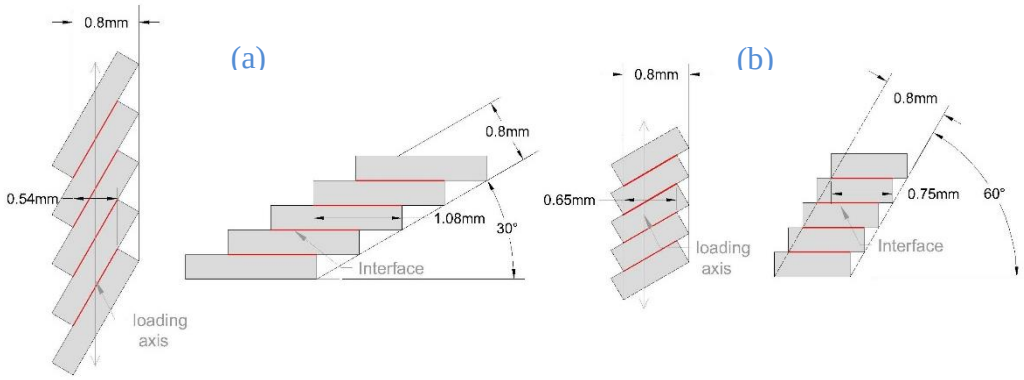

Figure 21 Representation of 30° (a) and 60° (b) microstruts. Conceptually, with a layer thickness of 0.3mm, the effective cross-section widths are 0.54mm and 0.65mm for the 30° and 60° microstruts when loaded axially.

4. Mesoscale

At this level, mostly geometric features are incorporated in the design, although the capability to introduce them in the design is not exclusive of powder bed fusion technologies, these manufacturing methods have shown probably the most versatile and controlled free forming capabilities for creating open-cell cellular metals. Thus it is meritorious that the geometric attributes are considered when designing cellular solids fabricated by powder bed fusion systems. In this context, the mechanical properties of the lattice are customized by modifications in the architecture of the unit-cell. The determinants at this level include stochasticity, nested hierarchical levels, aspect ratio, the Maxwell stability criterion, relative density, and auxetics; these factors may be considered as the major contributors to the mechanical properties of cellular solids. Noteworthy

is that changes in these determinants will inherently result in different cooling and solidification rates, with the possibility of substantial alterations in the microstructure (Kwon et al., 2003; Murr et al., 2010; Yang et al., 2012b). However, these effects and the following aspects can be compensated, up to certain grade, from the microscale determinants.

4.1. Stochasticity

Additive Manufacturing has made possible the fabrication of unit-cells in practically limitless shapes; however, the deformation mechanisms influencing the performance of the cellular solid are, in general, the same. The introduction of hierarchical levels is mostly what transforms a constituent solid into a metamaterial. One of the most general differentiation between cellular materials is that from observing its networking: stochastic or foams, and non-stochastic or lattices (Figure 22). Lattices were observed to fail in a more predictable manner while displaying more uniform properties, better structural performance, and more damage tolerance when compared to foams (Gorny et al., 2011; Wallach and Gibson, 2001).

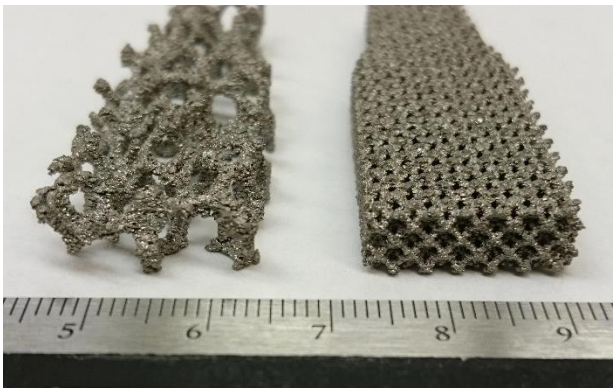

Figure 22 EBM fabricated Ti-6Al-4V cellular solids: foam (Left) and lattice (Right).

4.2. Nested Hierarchical Levels

The material phases in the microstructure can be seen as embedded levels in the unit-cell. It has been determined that nesting hierarchical levels improves the mechanical properties and enhances the energy absorption capabilities of cellular materials (Vigliotti and Pasini, 2013). Additionally, embedding hierarchical levels of unit-cells can constitute cellular solids with different and specific stages of response for superior damage tolerance. In the form of 3D hexagonal and 3D reentrant hexagonal, the lattice specimens for this study enclosed single-level unit-cells only (Figure 23).

4.3. Aspect ratio

The mechanical response of lattices also reacts to the aspect ratio of the unit-cell; research work suggests its influence on the compressive strength and stiffness, independently of the architecture of the unit-cell (Gümrük and Mines, 2013; Smith et al., 2013; Ushijima et al., 2011; Yang et al., 2012b). Similar to the slenderness ratio on microstruts, under compression, tall and narrow unit-cells are expected to display higher yield strengths when loaded vertically, but they are more likely to collapse by elastic buckling if they lack of proper lateral support. The designer should be aware of this instability in the unit-cell, despite it can be alleviated by the lateral support from the adjacent cells. The aspect ratio of the unit-cell in the designs presented herein was defined 1:1:1 (length:width:height), to avoid biased effects from this determinant, and maintaining a soft unit-cell with enough space for unrestraint deformations (Figure 23).

4.4. Maxwell stability criterion

Considering the type of forces developing in the microstruts, the unit-cells are typically referred as stretch-dominated, or bending-dominated (Ashby 2006), however, because the inherent unidirectionality of the stretch-dominated term, and the possibility of the microstruts acting under tension, or compression, the term might not be appropriated. In that manner, the deformation of these lattices are referred in this document as: *axially-dominated*. The unit-cells require to be analyzed and determined if they are kinematically stable and/or developing self-stress states, followed by resolving if they will behave as *structures* (axially-dominated), or as *mechanisms* (bending-dominated); however, by simply evaluating the *necessary* generalized Maxwell's criterion for 3D structures is enough to determine it for most of the configurations (Maxwell, 1864).

A generalized matrix approach on a generalized Maxwell stability criterion was presented by (Pellegrino and Calladine, 1986) to additionally detect the absence of kinematic equilibrium as another requirement for a rigid axially-dominated structure. The analysis also provides insight of how biased the structure is toward the axially-dominated threshold. Thus structural unit-cells are those with a value of $M \geq 0$ (Pellegrino and Calladine, 1986). The generalized Maxwell Criterion for 3D structures is given by:

$$M = b-3j+6$$

Where $M<0$ indicates that a unit-cell with b number of struts, j frictionless joints will collapse in mechanistic manner (bending-dominated). For simplicity purposes, we can identify that the axially-dominated unit-cells ($M \geq 0$, statically + kinematically determined) are those strictly formed from stiff triangles only, with no hinges on the sides.

The decision in selecting the hexagonal and re-entrant hexagonal polyhedron shapes as unit-cells for the design of the lattices being investigated is based on the understanding that hexagons

are the simplest symmetric mechanistic polygons where most of the design determinants herein can be addressed. While four and five sided closed polygons may seem simpler, no symmetric configurations capable of displaying auxetic behavior in 3D with inclined microstruts was found. The *necessary* Maxwell stability criterion for the both unit-cells herein investiged is M= -19 (b = 29, j = 18) (Figure 23).

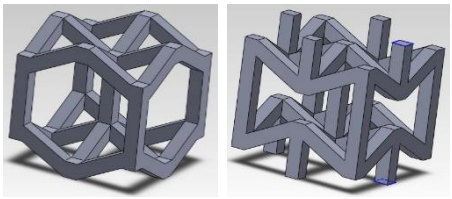

Figure 23 Examples of mechanistic unit-cells (M<0). Free-end struts (right) are considered part of another unit-cell.

Individual testing of microstruts displayed linear responses with practically null plasticity (Figure 20), thus, we could expect the response of the unit-cell to be also linear. However, because of the principles of the mechanistic deformation explained by Maxwell, the response of the hexagonal unit-cell displayed non-linear behavior. In this manner, aided by DIC, a stress-strain curve was obtained by measuring the strain of a single load cell at the center of the lattice, with a proportional point load of P/100 (P = total load on the lattice), corresponding to the outside face of the examined unit-cell (Figure 24); the recordings from testing displayed a non-linear response, best described by a parabola, according to the high R-value shown (Figure 25).

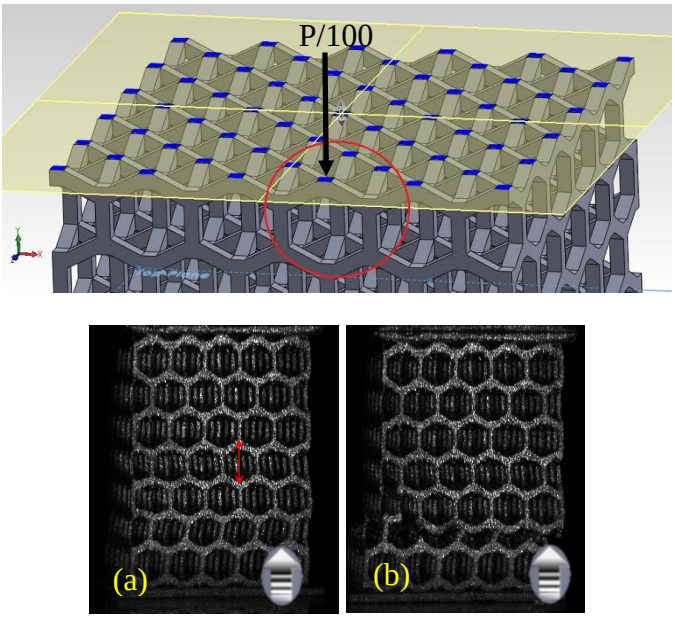

Figure 24 DIC images of 5mm hexagonal lattice: an instant before fracture (a) and after fracture (b). The double arrow at (a) indicates the initial position of the virtual extensometer.

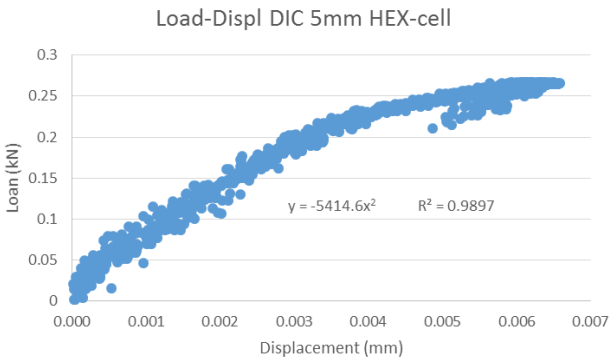

Figure 25 Non-linear stress-strain curve of a single 5mm hexagonal unit-cell during the compression test on the lattice.

Given that the Maxwell criterion considers frictionless joints, friction-equivalent expressions in function of the defined yield strength of the material at the node are still pending to develop to predicting the formation of plastic hinges, and optimizing the nodal geometry that permits it. This will derive in new ways to enhance the mechanistic deformation, material recovery, and specific energy.

The approach exposed by this stability criterion can be also applicable to molecular geometries. Therefore, considering a purely geometrical approach, the limited deformation capability of axially-dominated cellular metals can be increased by the inclusion of substantial amounts of material phases characterized by bending-dominated crystalline structures such as Hexagonal Close Packed. In this manner, we can compensate, or extend, the deformation capabilities of the cellular solids and their constituent solid materials by design approaches at different scale levels.

4.5. Auxetic

Since the first reported designed negative Poisson's ratio material by (Lakes, 1987), mostly polymers could be fabricated with this characteristic. These auxetic materials could still be considered rare, but now easier to design and fabricate thanks to AM technologies. Powder bed fusion systems make possible the fabrication of engineered metals with negative Poisson's ratio. As one of the most important strain relationships, the Poisson's ratio should be investigated separately given its directly proportional participation in stress-strain relationships. Materials displaying negative Poisson’s effect imply that their shear modulus is substantially larger than their bulk modulus, thus superior behavior against torsion, bending stiffness, energy absorption efficiency, and others is expected (Yang et al., 2012a). A variety of auxetic architectures can be developed to take advantage of its high shear modulus. Some auxetic geometries can experience different stress distribution modes as they are able to reconfigure themselves under loading; displaying an extra ultimate strength, or a completely different *stage* of mechanical behavior

(Figure 26 andFigure 28) (Lakes and Witt, 2002; Larsen et al., 1997; Smith et al., 2000; Warren, 1990; Yang et al., 2012a, p.).

During the compression test of 5mm reentrant hexagonal lattices, the axial and transverse strains were measured via DIC at an external unit-cell. The recordings initially displayed a linear negative Poisson's ratio of 0.21; a second non-linear transition zone from positive to negative; and a third and final linear segment with a positive Poisson's ratio of 0.06 before fracturing (Figure 26).

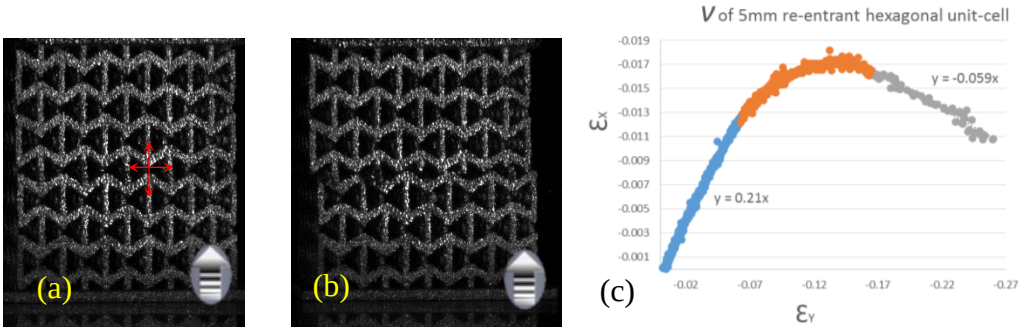

Figure 26 DIC images of a 5mm reentrant hexagonal lattice: an instant before fracture (a) and after fracture (b). The double arrows at (a) indicate the location of the virtual extensometers. Measured negative Poisson's ration at the unit-cell indicated by the extensometers (c).

4.6. Relative Density

Defined as the ratio of the density of the cellular solid divided by the density of its constitutive solid, the relative density has been found in many cases to be proportional to the elastic modulus and strength. This is the cornerstone of the widely and experimentally accepted Gibson and Ashby model for the mechanical properties of cellular solids (Ashby, 2006). However, this experimental relationship presents inaccuracies as the relative density increases (Liebenstein et al., 2016; Sing et al., 2016).

Equation 1. Gibson and Ashby model for E and σ. Where E is the Elastic Modulus, ρ is the density, $\boldsymbol{C}$ and $\boldsymbol{n}$ are experimental constants; $\mathbf{s}$ subscripts denote for solid

$$\frac{E}{E_s} = C\left(\frac{\rho}{\rho_s}\right)^n \quad ; \qquad \frac{\sigma}{\sigma_s} = C\left(\frac{\rho}{\rho_s}\right)^n$$

It is important to have in mind that focusing only in increasing the relative density to obtain stronger lattices, may lead to unexpected results and inefficient structures (Sing et al., 2016). In that manner, we could be incrementing the density by adding only idle material; it is only when conjugating the effect of effectively increasing the relative density with all variables discussed

herein, that the designer realizes about the complex optimization problem being addressed and whose objective function is to make the constitutive solid the most useful for energy management.

In this work, the relative density of the lattices being analyzed was defined by modifying the cubic size of its unit-cells only. In accordance with the Gibson-Ashby relationship, the denser lattices displayed higher strengths. The selected sizes of the unit-cells were 5mm, 6mm, and 7mm (Figure 27Figure 35).

Lattice	ρ* (gr/cm3)	Ult. Strength (kPa)
5mm HEX, 0.8mm strut	0.800	40,000
6mm HEX, 0.8mm strut	0.6	21,000
7mm HEX, 0.8mm strut	0.470	15,000
5mm RE-HEX, 0.8mm strut	1.130	35,000
6mm RE-HEX, 0.8mm strut	0.82	21,000
7mm RE-HEX, 0.8mm strut	0.65	13,000

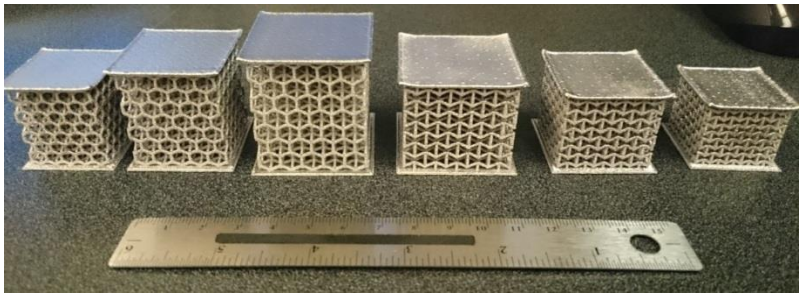

Figure 27 Averaged ultimate compressive strength of EBM Ti-6Al-4V Cellular solids with different densities fabricated at The W.M. Keck Center for 3D Innovation ("W.M. Keck Center for 3D Innovation," n.d.).

5. Macroscale

Similar to the mesoscale, the characteristics at the macroscale level may not be exclusive of EBM, but as mentioned before, it probably is one of the most versatile methods to fabricating cellular metals. One of the most useful and practical analyses that can be done on the performance of cellular materials, as a solid itself, is by scrutinizing its stress-strain curve to be able to interpret behaviors and diagnose the most convenient attributes to modify toward the expected performance (Figure 28). The determinants at this level include: lattice orientation, deformation mode, brittleness, recovery and unit-cell specifics. At this stage, because of the probably unknown boundary effects, it is recommended to proportionally estimate the required number of unit-cell

levels forming the lattice to withstand the loading. This is the convenient scale level for reverse engineering and material development.

The compressive response of cellular materials is ideally characterized by three major phases. First, an elastic region, up to the yielding point in which the microstruts start to buckle, fracture or yield. As the structure progressively collapses at nearly constant stress, the stress-strain curve displays a plateau; this second stage is often where the majority of the energy from loading might be absorbed. Once all the unit-cells levels have collapsed, the stress steeply rises, indicating the start of the densification stage, when the collapsed microstruts come in excessive contact and friction with each other, to ultimately deform, filling the remaining voids in the collapsed lattice (Ashby, 2006) (Figure 28).

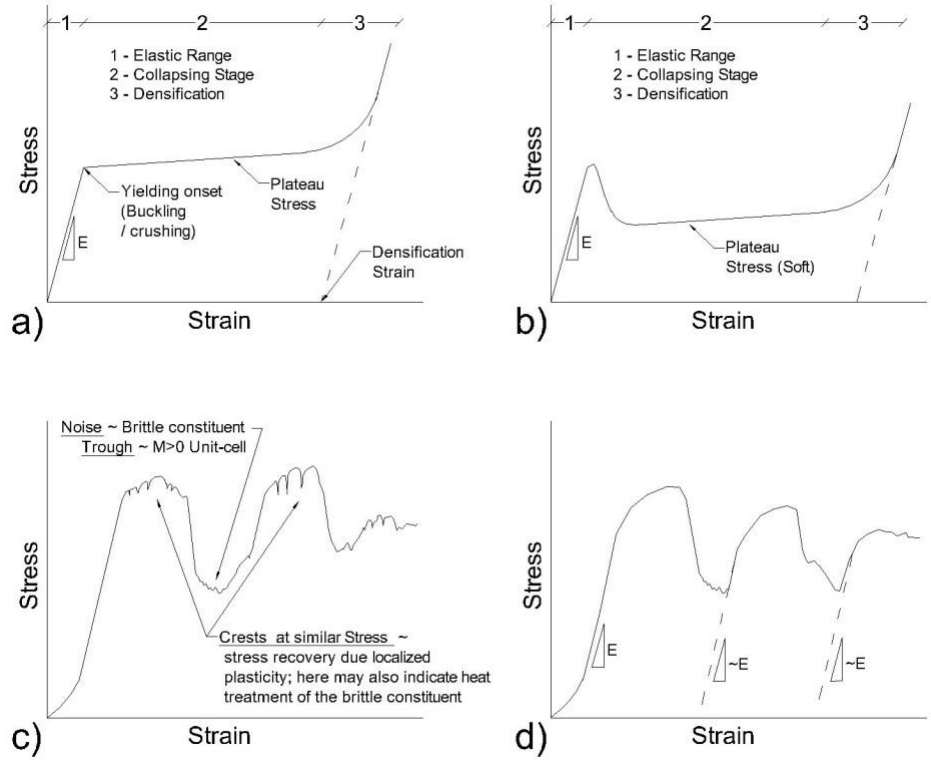

Figure 28 Representations of different compressive responses of cellular solids, highlighting behaviors originated by specific features. a) ideal 3-stages response of ductile, bending-dominated lattices ($M<0$); b) 3-stages response of brittle, axially-dominated lattices ($M\geq0$); c) expected response of lattices fabricated with brittle constituents, probably enhanced for plasticity by thermal treatment; d) Expected cyclic response of auxetic, self-bracing unit-cells, probably with some stress recovery and/or slightly local plasticity enhancement.

5.1. Lattice orientation

The overlapping effect inherent to powder bed fusion fabrication especially affects the properties of microstruts with oblique manufacturing angles (Figure 29). Orthogonally symmetric cells react stronger and stiffer when loaded parallel to the manufacturing direction, thus *sharper* shaped stress-strain curves are expected whereas shorter and longer curves are related to loads applied perpendicularly. Besides the unit-cell design, these step-like features can also result in the cellular solids with noticeable orthotropic properties (Figure 30). Noteworthy is to mention that for the purposes of energy absorption, a shorter and longer curve is generally preferred as the area underneath typically is larger compared to thin and tall curves (Cansizoglu et al., 2008).

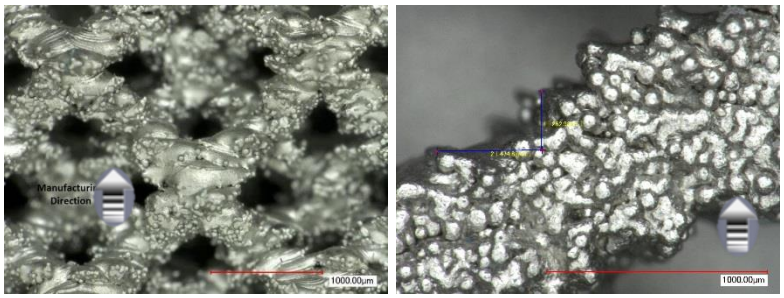

Figure 29 Node and microstruts in a lattice displaying the layering pattern, pores and sintered precursor (left). Close view of a ~60° microstrut in a hexagonal lattice, highlighting step-like features measuring 480µm long by 250µm tall approximately (right). 1mm scale marks.

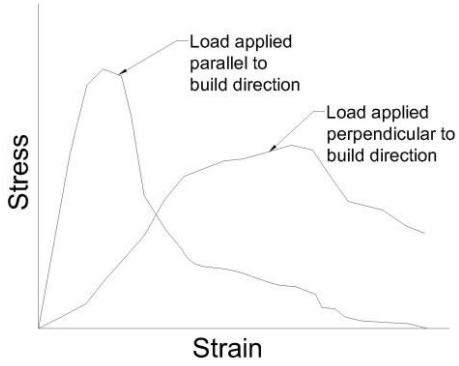

Figure 30 Schematic responses of orthogonally symmetric Cellular Solids to the loading direction.

5.2. Deformation mode

Lattices formed by axially-dominated unit-cells (M≥0) are normally stiffer and possess higher yield strengths when compared to bending-dominated lattices (M<0), however, they display a soft plateau stress when collapsing. Thus axially-dominated lattices are structurally more efficient, but bending-dominated are better performers for energy absorption purposes, as they display long plateau stress without the softening (Figure 28 and Figure 28). Further analysis of the *necessary* Maxwell stability criterion, for lattices to deform as structures, not as mechanisms, makes evident that only the unit-cell architectures, whose microstruts configuration is exclusively based on triangles, can create strictly axially-dominated lattices (Ashby, 2006; van der Giessen, 2011).

Being able to obtain a non-linear response due geometric features of a single unit-cell (Figure 25), the expected response of a cellular solid formed from linearly behaving members (Figure 20) constituting mechanistic unit-cells, is also non-linear. Noteworthy is the ability shown here of compensating for the lack of plasticity from the precursor material by creating cellular solids with a non-linear response, therefore enhancing the specific energy (Figure 31).

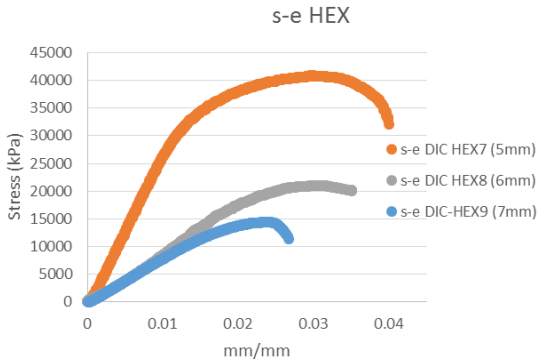

Figure 31 Compressive responses of hexagonal lattices with different densities. The non-linear response compensates for the lack of plasticity from the brittle microstruts with linear behavior.

5.3. Brittleness

A brittle constituent can be identified by several stress fluctuations in the collapsing stage. As the unit-cells progressively collapse in a catastrophic manner, the stress-strain curve resembles a noisy signal-like graph (Figure 28) (Cheng et al., 2012; Lorna J. Gibson and Michael F. Ashby, 1999). Furthermore, a deeper understanding and analysis on the constitutive solid and its relationship with these fluctuations could be helpful in the identification and quantification of material phase transformations occurred during the fabrication of after heat treatment, however, no methods were found yet. Despite the efforts at the different scale levels to maximize the non-linear behavior of lattices, to compensate for the lack of plasticity, a close view to the non-linear section of the stress-strain curve reveals a brittle behavior from the Ti-6Al-4V (Figure 32).

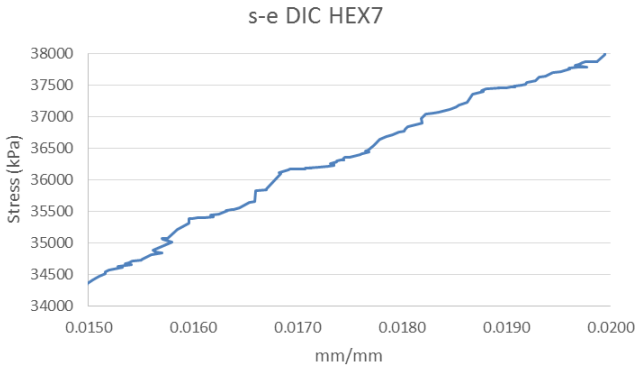

Figure 32 Residual brittleness in the non-linear response of a 5mm hexagonal lattice.

5.4. Recovery

Crest in the stress-strain curve normally describe the progressive collapse of groups of unit-cells, where each crest ends with the failure of one of these groups and the loading redistribution to another group, affecting a whole unit-cell level, or several unit-cells from various levels. For cellular solids progressively collapsing in a level-by-level basis, consecutive peaks failing to regain the previous maximum stress are indicators of a brittle structure whose cells are fracturing (Figure 28); whereas buckling microstruts in ductile structures come in contact and redistribute the stress without major ruptures. Constant stress from the plasticity in the buckling process, permit the next weakest level of cells to recover and withstand a second stress of similar magnitude (Figure 28). When manufacturing lattices made of constituents well known to be brittle, consecutive stress peaks of similar magnitude could also suggest a post-manufacturing heat treatment favoring ductility; this behavior could be investigated as indicator of the effectiveness of the treatment in phase transformations (Cheng et al., 2012; Gorny et al., 2011; Hernández-Nava et al., 2016).

The experimented lattices present an increasingly non-linear behavior as the unit-cell size decreased. Despite the microstructural and geometric design approaches that extended the deformation capability of the ductile-limited Ti-6Al-4V, the lattices failed in a brittle manner (Figure 36). The voids in the lattices were larger than the ultimate deformations from the microstruts, thus the stresses were not able to be relieved by contact between microstruts before fracturing. However, the strength recovering in the lattices of both configurations was perceived by the subsequent ultimate load of similar magnitude, supported by the next weakest unit-cells level. The slight decrement of peak loads can be approximated by a constant slope, and can act as an indicator of accumulated damage, proportional to the loading history. This is observed in most, but not all of the lattices, a larger sample size will reduce the uncertainty and may confirm the trends of cumulative damage for all unit-cell sizes (Figure 33).

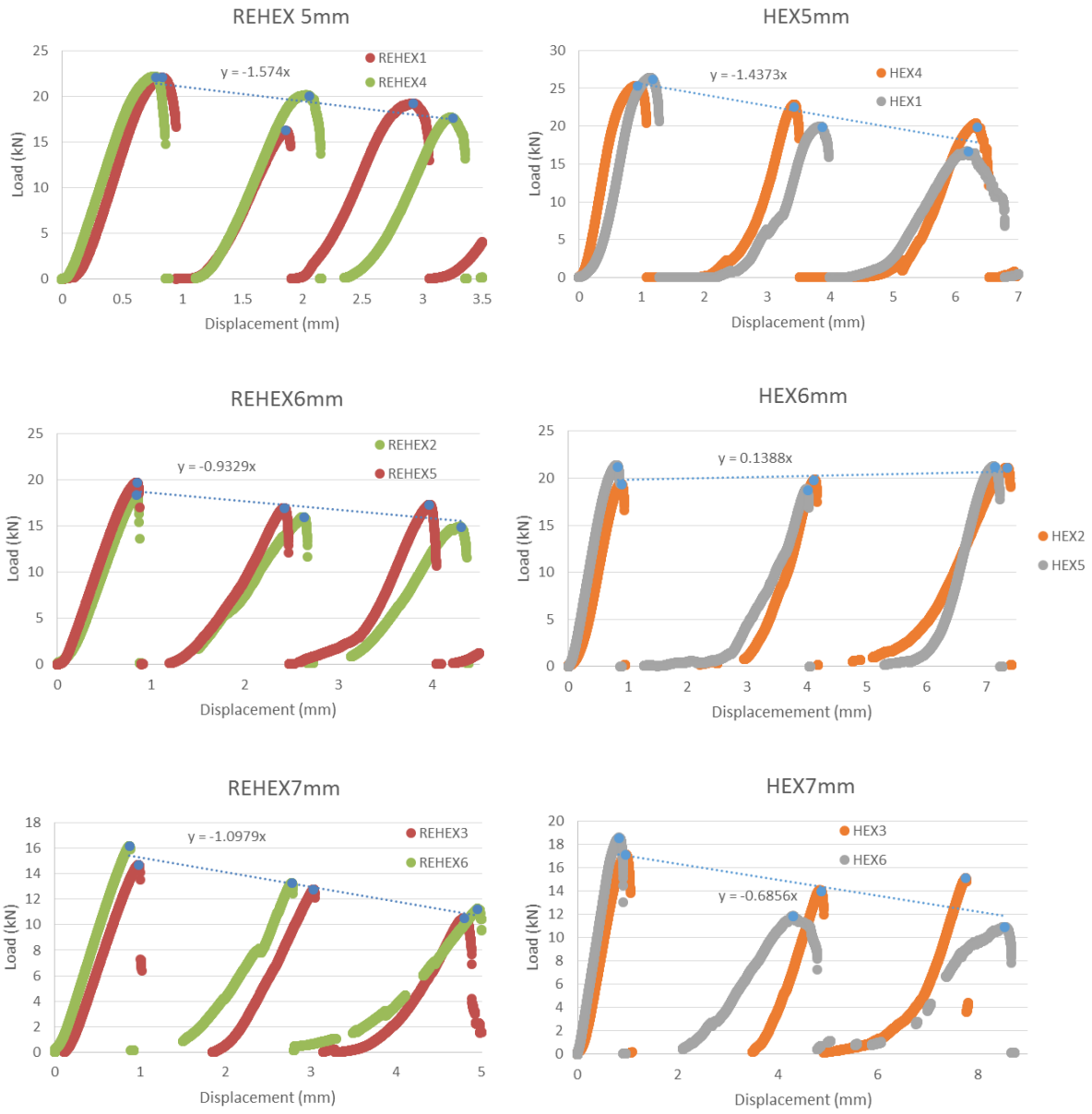

Figure 33 Progressive collapse of unit-cell levels in lattices displaying recovery and accumulated damage. Reentrant hexagonal lattices (left) and hexagonal lattices (right) at different unit-cell size. Two specimens of each size and configuration are displayed.

5.5. Unit-cell specifics

Microstruts fabricated with variable a cross section, specific local orientation, nodal geometry, re-entrant angles, multimaterial (Mireles, 2016), and others, are examples of more specific features that can be engineered for unit-cells with tailored response. These singular responses can also dictate particular trends on the stress-strain curve (Deshpande et al., 2001; Yang et al., 2012b). The contribution of these features should be analyzed independently such as in the case of unit-cells with auxetic behavior, where these cellular solids are normally stiffer and with higher structural efficiency (Figure 34).

In general, during the experiments, the reentrant hexagonal lattices displayed limited non-linear behaviors; moreover, they continued to follow the Gibson-Ashby relationship of higher strengths at higher specific densities, in unit-cells with the same configuration. However, it is important to note that, although the density of the lattice was increased by the reentrant sides of the hexagon, the amount of solid precursor material is essentially the same for hexagonal and reentrant hexagonal unit-cells of the same size; therefore, when selecting the proper unit-cell geometry, the relative density should not necessarily be considered as a major contributor of specific energy.

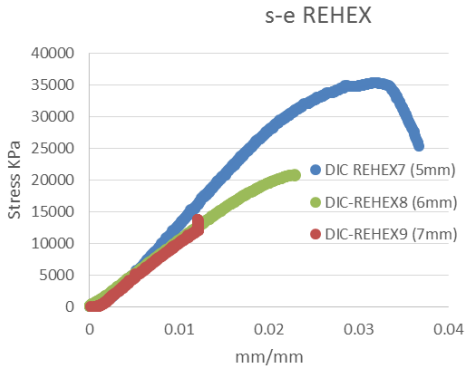

Figure 34 Compressive response of reentrant hexagonal lattices with different unit-cell sizes.

Experimental results from the compression tests revealed that the reentrant hexagonal lattices with large (6mm, 7mm) unit-cells were stiffer by approximately 10% and 25% respectively when compared to the hexagonal of the same size. The ultimate strength for both cell configurations was comparable within a 3%, however, the hexagonal lattices displayed considerably larger non-linear strains. For the unit-cell size of 5mm, the previous observation was reversed; the hexagonal lattice exhibited to be stiffer and stronger than the reentrant hexagonal, however, their strains were comparable within 10% (Figure 35). Turning into a purely geometrical approach, these results can be explained by reviewing how the load distributes throughout the structures: the reentrant hexagonal lattices develop a combined stress system of tension along the zigzagging microstruts and compression in the vertical microstruts, whereas the hexagonal lattices generate a purely compressive system. In a purely compressive system, all the microstruts react as columns, thus as

the unit-cell size increase, the unsupported length is also increased and critical instabilities are more likely arising, added to manufacturing defects, and the larger number of elements under compression in the hexagonal lattices.

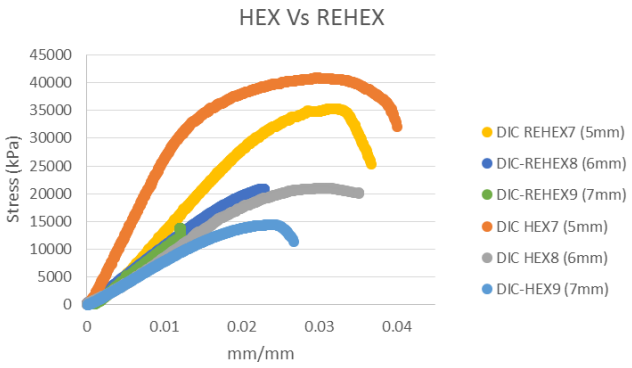

Figure 35 Stress-strain curves of hexagonal and reentrant hexagonal lattices at different unit-cell size.

Another interesting behavior of the auxetic structures is the capacity of containing the energy release from the failure. Despite the catastrophic brittle fracture, the re-entrant hexagonal lattices imploded, maintaining the specimen in place; whereas an explosion was characteristic of the sudden energy release events in the hexagonal lattices (Figure 36).

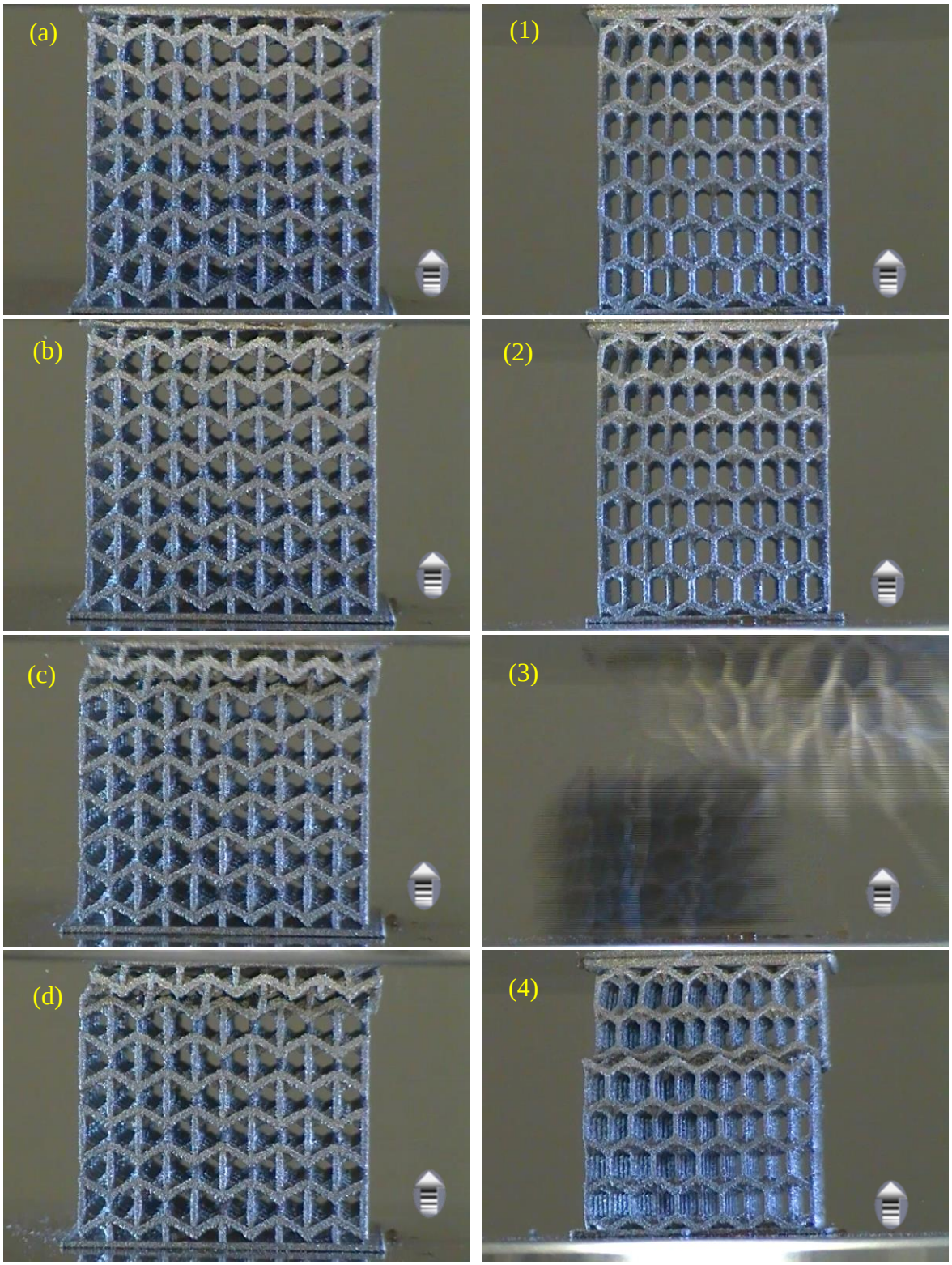

Figure 36 Lattices at different loading stages: unloaded (a, 1), an instant before failure (b, 2), the instant at failure (c, 3) and after failure (d, 4), (4) was replaced for image comparison. The energy releasing events of the two unit-cell configurations totally opposite (c, 3). (29 frames/s)

The reentrant hexagonal designs were expected to display a two-stage response. After the initial behavior shown here and completing a first deformation stage, a jaw-like feature was intended to lock the deformed unit-cell (Figure 37), creating a new nodal configuration and morphing the cell into four new, smaller, stiffer, and Poisson's-positive unit-cells, formed by four triangles each (Figure 37). It is important to note that these new unit-cells would neither comply with the Maxwell stability criterion to be defined as axially-dominated; this because of the square configuration of the four triangles arrangement from a top view (Figure 37). However, given that the loading would be distributed on the planes of the triangles, the expected response would tend more toward rigid. Most of the presented lattices fractured before the bite feature locked; the second stage of the response of these lattices could have been achieved by a design approach specifically aimed to enhance this required deformation, by means of any of the determinants previously discussed, such as creating nodes richer in alpha phase.

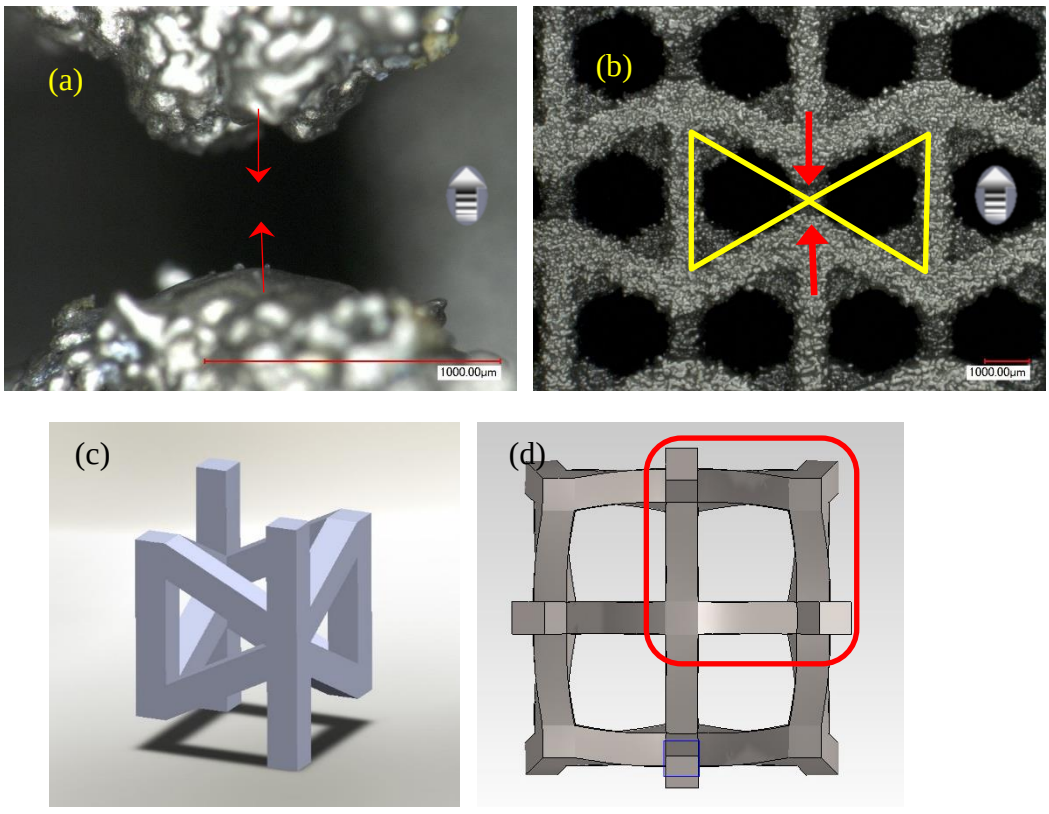

Figure 37 Jaw feature at the center of each reentrant unit-cell (a); representation of the expected unit-cell transformation (b); rendering of the new unit-cell after transformation (c); rendering of the top view of a deformed reentrant hexagonal unit-cell reconfigured into four new triangular unit-cells (d).

6. Remarks

Hierarchical levels in the microstructure can be controlled from the manufacturing settings by promoting the formation of convenient atomic arrangements in the solid. Mesoscale attributes are practically limited by imagination in the designing of unit-cells since almost any topology can now be introduced in the solid. Finally, at a macroscale, the response can be controlled by the quantity and arrangement of the unit-cells.

Such as the crystalline structures represent the minimum unit of volume containing the structural and geometric information to characterize solids, the unit-cell is similar for the cellular materials, thus it is expected that the topology at the mesoscale level contributes the most toward the overall response.

The keystone of the present work is to encourage and prioritize the comprehensive knowledge of the cellular metals before addressing their design. Thus, in developing a more structured reasoning, the multiple factors contributing to the performance of these materials have been investigated according to scale (Figure 38). In this manner, after the understanding of the service requirements, it is advisable to start the conceptual design at the mesoscale, where the determinants are highly controlled and are major contributors to the performance of the cellular solid. For example, where energy absorption in an aggressive environment is of special interest, and following the determinants previously exposed, a cellular metal could be defined as a lattice, with a primary level of unit-cells with $M<0$ embedding a softer $M<<0$ hierarchical level for the abrupt deceleration of initial impacts and energy dispersion respectively, 1:1 aspect ratio, non-auxetic with optimal density. Once the unit-cell has been conceptualized, the design is enhanced at the microscale where the variables are less controlled; thus, EBM Grade 2 Titanium may be a good alternative given its formability, lightweight, and corrosion resistance. In this case, the effects of manufacturing parameters shall be analyzed for the possibility to promoting the stiffer β-phase in the primary unit-cells, and conserve the most α-phase in the secondary level. The degradation of the mechanical properties could be addressed by either oversizing the microstruts, or by obtaining all-inclusive material properties from specimens that include manufacturing defects. Outcomes from the manufacturing process are recommended to follow a more statistical approach, especially if the manufacturing systems serve different operations. As the common file format for AM system, the effects of *.STL* should be addressed together with the mechanical properties degradation until a more precise file format becomes dominant. At the macroscale the lattice manufacturing direction should be parallel to the direction of the main load for larger deformations. Finally, the response of the cellular solid can be interpreted, and the undesirable performances addressed to start a reverse engineering process, including the addition of new unit-cell levels for new response stages.

Determinant	Specific energy enhancement:	Variables
Microscale		
Manufacturing Technology	EBM builds normally display lager elongation that SLM.	Powder bed fusion technologies.
File Format	.stl is currently the common file in additive manufacturing technologies. It implies discretize geometries into triangles that may limit the design and introduce flaws and defects.	.stl, CAD, others available.
Constituent solid	Prefer those with atomic structures recognized to deform as mechanisms and similar life cycles.	Available powder precursors and their condition.
Manufacturing Parameters	Increase energy and time of exposure for higher density, therefore less early failure. Control settings that produce ductile material phases.	power, time, layer thickness.
Manufacturing Process	Procure cooling and solidification rates that do not alter, but promote microstructures with ductile phases.	manufacturing layout, self-geometry, supports, process interruptions.
Degradation of the Mechanical Properties	Compensate for the degradation of mechanical properties due scale factor, mostly.	scale factor, slenderness ratio, layer thickness, orientation, CAD draft errors.
Mesoscale		
Stochasticity	lattices are normally more damage tolerant, more uniform properties, and fail in a more controllable manner	foams, lattices.
Nested Hierarchical Levels	Include nested levels that enhance energy absorption.	number and individual performance of nested levels.
Aspect ratio	Prefer Slenderness ratios close to 1.	length, width, height, slenderness ratio, effective length.
Maxwell Stability Criterion	M<<0	number of joints, number of self-stress states, number of mechanisms.
Auxetic	Negative Poisson effect normally increases stiffness; as a general advice, avoid purely auxetic structures.	re-entrant angles, unrestricted motion.
Relative density	Density is normally proportional to strength, but not necessarily a major contributor for specific energy.	nodal geometry, microstrut aspect and slenderness ratios.
Macroscale		
Lattice Orientation	Prefer layering deposition direction to be perpendicular to the expected loadings.	x, y, z
Deformation Mode	Prefer bending-dominated lattices.	M, nodal geometry, microstrut aspect and slenderness ratios.
Brittleness	Avoid geometry brittleness.	Constituent precursor.
Recovery	After the collapse of a unit-cells level, the stress recovery will extend specific energy.	Constituent precursor, topology, post-manufacturing treatments.
Unit-cell specific	uniquenesses of unit-cells can benefit specific energy.	Imagination.

Figure 38 Summary of the determinants of design followed in a multiscale analysis.

In the reviewed literature, expressions are found addressing some of the relationships experimentally evidenced in this study, however, their scope is somehow encompassed by the specialization of the researcher. Thus, the development and agreement of acceptable quantitative expressions for the experimentally exposed relationships integrated into a design process are vital in the fabrication of uniform and reliable cellular solids (e.g. Strength in function of volume/beam power/amount of ductile phase, etc.). It is important to highlight that the concepts exposed here can be also valid for materials other than metals, such as for polymers with large, highly deformable molecular geometries; where the determinants proper from the AM technology used will require further study.

Powder bed fusion provides the opportunity for practically unlimited unit-cell designs. The design of cellular metals, as a discipline, is not close yet to a standardized system of theories, methods; however, with the multiscale analysis approach herein, the identification of determinants of design has been structured. Nonetheless, it is still on the experience, availability and convenience of the designer to discern which of the presented attributes to customize toward achieving the expected lattice response.

In an effort to reduce the uncertainty among the determinants that are poorly controlled, the creation of databases and sensitivity analyses is vital for a statistical approach. Furthermore, computational mechanics boosted by these databases will empower the designers to accurately develop multivariable optimization methods to objectively weigh, evaluate and select the design determinants.

Future work includes the development of quantitative expressions for specific energy in function of the determinants discussed, the expansion of this approach to structures with different precursor materials, multiple hierarchical levels, as well as behavior under dynamic loads.

7. Acknowledgements

This research is partially funded by the National Science Foundation, Grant 1405526. Specimens manufactured by Israel Segura from the W.M. Keck Center for 3D Innovation.

8. References

Ashby, M.., 2006. The properties of foams and lattices. Philos. Trans. R. Soc. Math. Phys. Eng. Sci. 364, 15–30. doi:10.1098/rsta.2005.1678

Cansizoglu, O., Harrysson, O., Cormier, D., West, H., Mahale, T., 2008. Properties of Ti–6Al–4V non-stochastic lattice structures fabricated via electron beam melting. Mater. Sci. Eng. A 492, 468–474. doi:10.1016/j.msea.2008.04.002

Cheng, X.Y., Li, S.J., Murr, L.E., Zhang, Z.B., Hao, Y.L., Yang, R., Medina, F., Wicker, R.B., 2012. Compression deformation behavior of Ti–6Al–4V alloy with cellular structures fabricated by electron beam melting. J. Mech. Behav. Biomed. Mater. 16, 153–162.

doi:10.1016/j.jmbbm.2012.10.005
Deshpande, V.S., Ashby, M.F., Fleck, N.A., 2001. Foam topology: bending versus stretching dominated architectures. Acta Mater. 49, 1035–1040. doi:10.1016/S1359-6454(00)00379-7
Gong, H., Rafi, K., Starr, T., Stucker, B., 2013. The Effects of Processing Parameters on Defect Regularity in Ti-6Al-4V Parts Fabricated By Selective Laser Melting and Electron Beam Melting, in: ResearchGate. Presented at the 24th Annual International Solid Freeform Fabrication Symposium.
Gorny, B., Niendorf, T., Lackmann, J., Thoene, M., Troester, T., Maier, H.J., 2011. In situ characterization of the deformation and failure behavior of non-stochastic porous structures processed by selective laser melting. Mater. Sci. Eng. A 528, 7962–7967. doi:10.1016/j.msea.2011.07.026
Gümrük, R., Mines, R.A.W., 2013. Compressive behaviour of stainless steel micro-lattice structures. Int. J. Mech. Sci. 68, 125–139. doi:10.1016/j.ijmecsci.2013.01.006
Hernández-Nava, E., Smith, C.J., Derguti, F., Tammas-Williams, S., Leonard, F., Withers, P.J., Todd, I., Goodall, R., 2016. The effect of defects on the mechanical response of Ti-6Al-4V cubic lattice structures fabricated by electron beam melting. Acta Mater. 108, 279–292. doi:10.1016/j.actamat.2016.02.029
Kwon, Y.W., Cooke, R.E., Park, C., 2003. Representative unit-cell models for open-cell metal foams with or without elastic filler. Mater. Sci. Eng. A 343, 63–70. doi:10.1016/S0921-5093(02)00360-X
Lakes, R., 1987. Foam structures with a negative Poisson's ratio. Science 1038–1040.
Lakes, R.S., Witt, R., 2002. Making and characterizing negative Poisson's ratio materials. Int. J. Mech. Eng. Educ. 30, 50–58.
Larsen, U.D., Sigmund, O., Bouwstra, S., Larsen, U.D., Sigmund, O., Bouwstra, S., 1997. Design and fabrication of compliant micromechanisms and structures with negative Poisson's ratio. E E E J. Microelectromechanical Syst. 6, 99–106. doi:10.1109/84.585787
Liebenstein, S., Sandfeld, S., Zaiser, M., 2016. Modelling Elasticity of Open Cellular Foams: Size Effects and Disorder. ArXiv Prepr. ArXiv160403589.
Lorna J. Gibson, Michael F. Ashby, 1999. Cellular Solids: Structure and Properties, Second. ed. Cambridge University Press.
Maxwell, J.C., 1864. L. On the calculation of the equilibrium and stiffness of frames. Philos. Mag. Ser. 4 27, 294–299. doi:10.1080/14786446408643668
Mireles, J., 2016. Joining of Metallic Structures Using Powder Bed Fusion Additive Manufacturing Technology, in: Solid Freeform Fabrication Symposium. Presented at the SFFS, Austin, TX.
Murr, L.E., Gaytan, S.M., Medina, F., Lopez, H., Martinez, E., Machado, B.I., Hernandez, D.H., Martinez, L., Lopez, M.I., Wicker, R.B., Bracke, J., 2010. Next-generation biomedical implants using additive manufacturing of complex, cellular and functional mesh arrays. Philos. Trans. Math. Phys. Eng. Sci. 368, 1999–2032.
Murr, L.E., Martinez, E., Amato, K.N., Gaytan, S.M., Hernandez, J., Ramirez, D.A., Shindo, P.W., Medina, F., Wicker, R.B., 2012. Fabrication of Metal and Alloy Components by Additive Manufacturing: Examples of 3D Materials Science. J. Mater. Res. Technol. 1, 42–54. doi:10.1016/S2238-7854(12)70009-1
Murr, L.E., Quinones, S.A., Gaytan, S.M., Lopez, M.I., Rodela, A., Martinez, E.Y., Hernandez, D.H., Martinez, E., Medina, F., Wicker, R.B., 2009. Microstructure and mechanical behavior of Ti–6Al–4V produced by rapid-layer manufacturing, for biomedical applications. J. Mech. Behav.

Biomed. Mater. 2, 20–32. doi:10.1016/j.jmbbm.2008.05.004
Paul, R., Anand, S., 2015. A new Steiner patch based file format for Additive Manufacturing processes. Comput.-Aided Des. 63, 86–100. doi:10.1016/j.cad.2015.01.002
Pellegrino, S., Calladine, C.R., 1986. Matrix analysis of statically and kinematically indeterminate frameworks. Int. J. Solids Struct. 22, 409–428. doi:10.1016/0020-7683(86)90014-4
Sing, S.L., Yeong, W.Y., Wiria, F.E., Tay, B.Y., 2016. Characterization of Titanium Lattice Structures Fabricated by Selective Laser Melting Using an Adapted Compressive Test Method. Exp. Mech. 56, 735–748. doi:10.1007/s11340-015-0117-y
Smith, C.W., Grima, J.N., Evans, K.E., 2000. A novel mechanism for generating auxetic behaviour in reticulated foams: missing rib foam model. Acta Mater. 48, 4349–4356. doi:10.1016/S1359-6454(00)00269-X
Smith, M., Guan, Z., Cantwell, W.J., 2013. Finite element modelling of the compressive response of lattice structures manufactured using the selective laser melting technique. Int. J. Mech. Sci. 67, 28–41. doi:10.1016/j.ijmecsci.2012.12.004
Tsopanos, S., Mines, R.A.W., McKown, S., Shen, Y., Cantwell, W.J., Brooks, W., Sutcliffe, C.J., 2010. The Influence of Processing Parameters on the Mechanical Properties of Selectively Laser Melted Stainless Steel Microlattice Structures. J. Manuf. Sci. Eng. 132, 041011–041011. doi:10.1115/1.4001743
Ushijima, K., Cantwell, W.J., Chen, D.H., 2013. Prediction of the mechanical properties of micro-lattice structures subjected to multi-axial loading. Int. J. Mech. Sci. 68, 47–55. doi:10.1016/j.ijmecsci.2012.12.017
Ushijima, K., Cantwell, W.J., Mines, R. a. W., Tsopanos, S., Smith, M., 2011. An investigation into the compressive properties of stainless steel micro-lattice structures. J. Sandw. Struct. Mater. 13, 303–329. doi:10.1177/1099636210380997
van der Giessen, E., 2011. Materials physics: Bending Maxwell's rule. Nat. Phys. 7, 923–924. doi:10.1038/nphys2146
Vigliotti, A., Pasini, D., 2013. Mechanical properties of hierarchical lattices. Mech. Mater. 62, 32–43. doi:10.1016/j.mechmat.2013.03.003
Wang, X.J., Zhang, L.C., Fang, M.H., Sercombe, T.B., 2014. The effect of atmosphere on the structure and properties of a selective laser melted Al–12Si alloy. Mater. Sci. Eng. A 597, 370–375. doi:10.1016/j.msea.2014.01.012
Warren, T.L., 1990. Negative Poisson's ratio in a transversely isotropic foam structure. J. Appl. Phys. 67, 7591–7594. doi:10.1063/1.345826
W.M. Keck Center for 3D Innovation [WWW Document], n.d. URL http://keck.utep.edu/
Yang, L., Cormier, D., West, H., Harrysson, O., Knowlson, K., 2012a. Non-stochastic Ti–6Al–4V foam structures with negative Poisson's ratio. Mater. Sci. Eng. A 558, 579–585. doi:10.1016/j.msea.2012.08.053
Yang, L., Harrysson, O., West, H., Cormier, D., 2012b. Compressive properties of Ti–6Al–4V auxetic mesh structures made by electron beam melting. Acta Mater. 60, 3370–3379. doi:10.1016/j.actamat.2012.03.015
Zhu, F., Lu, G., Ruan, D., Wang, Z., 2010. Plastic Deformation, Failure and Energy Absorption of Sandwich Structures with Metallic Cellular Cores. Int. J. Prot. Struct. 1, 507–541. doi:10.1260/2041-4196.1.4.507